A new type of cobalt-deposited titanate nanotubes for enhanced photocatalytic degradation of phenanthrene

Xiao Zhao [a], Zhengqing Cai [a], Ting Wang [b], S.E. O'Reilly [c], Wen Liu [a,b,*], Dongye Zhao [a,*]

[a] Environmental Engineering Program, Department of Civil Engineering, Auburn University, Auburn, AL 36849, USA
[b] The Key Laboratory of Water and Sediment Sciences, Ministry of Education, Department of Environmental Engineering, Peking University, Beijing 100871, China
[c] Bureau of Ocean Energy Management, GOM Region, Office of Environment, New Orleans, LA 70123-2394, USA

ARTICLE INFO

ABSTRACT

We prepared and characterized a new type of photocatalyst, referred to as cobalt-deposited titanate nanotubes, using TiO_2 (P25) as the precursor through a two-step process (hydrothermal reaction at 150 °C followed by calcination at 600 °C). The optimal catalyst (Co-TNTs-600) was obtained at a Co loading of 2.26 wt.% and calcination temperature of 600 °C. The catalyst can effectively catalyze photodegradation of phenanthrene (a model polycyclic aromatic hydrocarbon) under simulated solar light. The pseudo first-order rate constant was determined to be $0.39\,h^{-1}$, which is about 10 times that of the conventional photocatalyst TiO_2. TEM, XRD and XPS analyses indicate that Co-TNTs-600 is a composite nanomaterial containing titanate, anatase and CoO crystals. The hydrothermal treatment converts TiO_2 into tubular, multilayered titanate nanotubes, allowing for incorporation Co(II) ions on the matrices. The subsequent calcination partially transforms titanate into anatase and the adsorbed Co^{2+} ions into CoO. UV–vis DRS spectra suggest that the absorption edge of Co-TNTs-600 shifts to the visible light region compared to P25 and un-calcined TNTs, and the new catalyst displays a narrower optical energy band of 2.8 eV compared to 3.2 eV for P25 and 3.4 eV for TNTs. The incorporated CoO acts as an electron transfer mediator, which prevents the recombination of hole-electron pairs created mainly by anatase under solar irradiation. In addition, Co-TNTs-600 exhibits good reusability and can be gravity-separated and reused in multiple cycles of operations for phenanthrene photodegradation. This new catalyst appears promising for catalyzing photodegradation of persistent polycyclic aromatic hydrocarbons.

© 2016 Elsevier B.V. All rights reserved.

1. Introduction

With increasing water pollution and growing energy demand, low-energy water treatment technologies become more and more appealing [1]. As such, catalytic photodegradation of various pollutants using solar irradiation has elicited great interest in recent years [2]. Traditionally, TiO_2-based materials have been the most widely used photocatalysts, and have been found effective in a variety of environmentally related uses, such as solar-driven hydrogen production, and photocatalytic decomposition and adsorption of organic contaminants [3–7].

TiO_2 is a typical *n*-type semiconductor with relatively large band gaps. The band gaps for the three main crystal phases, i.e., anatase,

rutile and brookite, are 3.2, 3.0 and 3.2 eV, respectively [6]. Although TiO_2 can effectively utilize UV light, its large band gaps limit its optical absorption in the solar spectrum, which consists of UV, visible and infrared (IR) radiations with a relative energy distribution of ~5%, 43% and 55%, respectively [8,9]. As a result, a great deal of effort has been devoted to improving the visible light absorption of TiO_2. While nanoscale TiO_2 has shown to offer improved catalytic activity, the sedimentation characteristics limit the separation from water and reuse of the spent catalyst [10].

Of various modifications, one-dimensional titanate nanotubes (TNTs) synthesized by hydrothermal treatment of TiO_2 have gained significant attention in recent years [5,10–12]. TNTs can serve as excellent adsorbents for heavy metals owing to their high specific area, great ion-exchange properties, easy solid-liquid separation and abundant functional groups. However, TNTs have been found to be poor photocatalysts despite their high surface area and crystalline structure due to the rapid electron-hole recombination rate upon excitation under illumination [13–15]. Therefore,

researchers have studied various approaches to inhibit the electron-hole recombination, including calcination [16,17], H_2O_2 treatment [18], acid treatment [19], and surface modification using non-metals such as C, F and P [13,20] or metals such as Fe, Cu, Pd, and W [21–23]. Of these approaches, metal doping/deposition appears very promising. An appropriate metal dopant can not only inhibit the recombination of electron-hole pairs, but also facilitate absorption of visible light by narrowing the absorption band gaps. Cobalt is one of the commonly used dopant for modifying TiO_2, and cobalt oxides have narrower band gaps (e.g., ~2.4 eV for CoO and 2.19 eV for Co_3O_4) [24,25]. For instance, cobalt oxide/TiO_2 composite showed much improved photo-activity for organic compounds and H_2 production rate than plain TiO_2 [26–28]. However, cobalt as a potential dopant for TNTs has not been studied.

Polycyclic aromatic hydrocarbons (PAHs) are produced during incomplete combustion of fossil fuels, and important components of crude oil [29,30]. Due to their toxic, mutagenic and carcinogenic properties, PAHs represent a major environmental concern associated with oil spill, discharge and seepage, and thus, have been classified as the priority pollutants by US EPA [31]. In addition, PAHs (e.g., phenanthrene, anthracene, and pyrene) are rather persistent to photodegradation under solar light [32]. PAHs can absorb light in the UV regions, and then be transformed into excited PAH molecules and photo-oxidized [33]. Phenanthrene is one of the most commonly detected PAHs, consisting of three fused benzene rings, it is fairly resistant to natural photodegradation, and thus, has been often used as a prototype PAH for photolysis study [34–36].

The overall goal of this work was to develop and test a new type of cobalt-deposited TNTs (Co-TNTs) for efficient photodegradation of PAHs under solar light. The specific objectives were to: (1) develop an optimized hydrothermal-calcination method for preparing the desired catalyst, (2) test the effectiveness of the catalyst for phenanthrene photodegradation, and (3) elucidate the mechanisms for enhanced photocatalytic activity by characterizing the morphology, crystal phases and compositions of Co-TNTs.

2. Experimental

2.1. Chemicals

All chemicals used in this study were of analytical grade or higher. TiO_2 nanoparticles (P25, 80% anatase and 20% rutile) were purchased from Degussa Corporation (Germany) and were used as the precursor for TNTs. $CoCl_2 \cdot 6H_2O$, NaOH, methanol (HPLC grade), dichloromethane (GC grade) and absolute ethanol were obtained from Acros Organics (Fair Lawn, NJ, USA). Terephthalic acid was purchased from Alfa Aesar (Ward Hill, MA, USA) for hydroxyl radical detection. Deionized (DI) water (Millipore Co., 18.2 MΩ cm) was used to prepare all solutions. Phenanthrene (the model PAH) was purchased from Alfa Aesar (Ward Hill, MA, USA), and was dissolved in methanol to form a stock solution of 2 g L^{-1}.

2.2. Synthesis of Co-deposited TNTs

First, Co-TNTs were synthesized through a one-step hydrothermal method. In brief, 0.1, 0.2, 0.4 or 0.6 g $CoCl_2 \cdot 6H_2O$ was mixed with 1.2 g of the TiO_2 nanoparticles in a beaker with 20 mL DI water. The mixtures were magnetically stirred for 30 min and sonicated for another 30 min. Then, a NaOH solution (prepared with 29 g NaOH in 47 mL DI water) was added dropwise into each mixture in ca. 5 min, and then sonicated for another 60 min. Afterwards, each mixture was transferred into a Teflon reactor with stainless steel coating, and then purged with pure N_2 for 10 min to remove dissolved oxygen. Then, the reactors were heated at 150 °C for 48 h to complete the hydrothermal reaction. The resulting blue

precipitates were separated and washed with DI water to neutral and then oven-dried at 80 °C for 4 h. The as-prepared materials are denoted as Co-TNTs for typographical convenience.

The Co loadings on Co-TNTs were determined according to EPA Method 3050B [37]. Briefly, 0.2 g each of the materials was dispersed into 20 mL of concentrated nitric acid (65%) and shaken for 24 h, and the resulting solution was diluted 10 times and then analyzed for Co on an inductively coupled plasma-optical emission spectroscopy (ICP-OES, 710-ES, Varian, USA). Subsequently, the Co-TNTs were calcined at 400, 600 or 800 °C in a muffle furnace for 3 h, and the resultant catalysts are denoted as Co-TNTs-xxx (xxx indicates the calcination temperature). The photocatalytic activities of the materials prepared with different Co loadings and calcination temperatures were then tested to optimize the recipe. For comparison, neat TNTs were also synthesized following the traditional hydrothermal method without Co loading [38,39], where 1.2 g TiO_2 (P25) and 10 M NaOH were mixed and heated at 130 °C for 72 h. In selected cases, the TNTs were calcined at 600 °C for 3 h, and the calcined TNTs are designated as TNTs-600.

2.3. Material characterizations

The morphology of material was analyzed using Tecnai30 FEG transmission electron microscopy (TEM, FEI, USA) operated at 300 kV, and energy dispersive spectra (EDS) of the materials were obtained at the same time. The crystal phase of the sample was obtained by means of a Bruker D2 phaser X-ray diffractometer (XRD, Bruker AXS, Germany) using Cu $K\alpha$ radiation (λ = 1.5418 Å) at a scan rate (2θ) of 4°/min. AXIS-Ultra X-ray photoelectron spectroscopy (XPS, Kratos, England) analysis was performed to determine the elemental composition and oxidation sate of materials using Al $K\alpha$ X-ray at 15 kV and 15 mA. The standard C 1s peak (Binding energy, E_b = 284.80 eV) was used to eliminate the static charge effects. The Brunauer-Emmett-Teller (BET) surface area was measured on an ASAP 2010 BET surface area analyzer (Micromeritics, USA) in the relative pressure range of 0.06–0.20. Pore size distribution was obtained following the Barret-Joyner-Halender method. Nitrogen adsorption volumes at the relative pressure of 0.99 were used to determine the pore volumes and the average pore diameters. Diffuse reflectance UV–vis absorption spectra (UV-DRS) of the materials were obtained using a UV-2400 spectrophotometer (Shimadzu, Japan). $BaSO_4$ powder was used as the reference at all energies (100% reflectance) and the reflectance measurements were converted to absorption spectra using the Kubelka-Munk function. The sedimentation rate tests of the materials were evaluated following the UV absorbance of the particle suspensions using a UV–vis spectrophotometer (UV1800, Shimadzu, Japan) (the particles were first dispersed in DI water with sonication) [10].

2.4. Photocatalytic degradation

Fig. S1 in Supplementary data (SD) shows the experimental setup for the photodegradation of phenanthrene, which includes a sealed glass photo-reactor (volume = 250 mL) with a quartz cover, an Oriel Sol 1A solar simulator (Newport, USA) with a 450 W xenon lamp, a water circulating system and a magnetic stirrer. The solar irradiation was set at of 85 ± 0.5 mW/cm^2 (AM 1.5G). The reactor temperature was maintained at 25 ± 0.2 °C through the circulating water.

Photocatalytic degradation kinetic tests were carried out with various materials under the simulated solar light. Specifically, 200 μg/L of phenanthrene and 1.0 g /L of a given material were loaded in the photo-reactor. The mixture was stirred for 2 h in dark to reach the phenanthrene adsorption equilibrium. Afterwards, the reactor was subjected to the solar irradiation. Water samples (1 mL each) were taken at predetermined times and imme-

diately centrifuged at 8000 rpm (6400 g-force) for 10 min. The supernatant was then mixed with methanol at 1:1 (v/v) ratio, and then analyzed for phenanthrene using an Agilent 1260 Infinity high performance liquid chromatography (HPLC) system equipped with a Poroshell 120 E C-C18 column (50 × 4.6 mm, 2.7 μm). The column temperature was held constant at 30 °C, and the mobile phase was comprised of acetonitrile and water at 70:30 (v/v) and at a flow rate of 1 mL min^{-1} in the isocratic mode. The eluate was analyzed with a UV diode array detector at 254 nm. The detection limit for phenanthrene was ~1 μg/L. Control tests were conducted in the absence of any catalysts but under otherwise identical conditions.

To determine the degradation intermediates, samples (100 mL each) were collected at 1, 3, and 6 h. Following centrifugation, each sample was extracted using 10 mL dichloromethane in 125 mL separatory funnels. The organic phase was collected and treated with anhydrous Na$_2$SO$_4$ to remove any water. Upon filtering with 0.22 μm Polytetrafluoroethylene (PTFE) membrane, the solvent was analyzed for various organic compounds using a GC–MS system (Agilent 7890A GC with 5975C Series mass spectrometry) equipped with an Agilent DB EUPAH column (121–9627, 20 m × 180 μm × 0.14 μm). The GC was operated in the full scan mode. The injection was carried out in the splitless mode (2.0 μL) at 300 °C. The oven temperature was programmed from 40 °C (1 min hold), and then increased to 300 °C at a ramping rate of 8 °C/min and held for 10 min.

Based on the screening tests, Co-TNTs-600, the most active catalyst prepared with 2.26 wt.% of Co loading and at a calcination temperature of 600 °C, was further tested for reusability. After an adsorption-photocatalysis cycle, the catalyst was recovered by filtering the suspension using a 0.22 μm PTFE membrane, and then reused by repeating the same adsorption-photodegradation cycle. Separate tests indicate that air-drying the catalyst had no effect on its catalytic activity.

The zero-order and first-order kinetic models are tested to interpret the kinetic data [40,41]:

$$C_0 - C_t = k_0 t \tag{1}$$

$$\ln\left(\frac{C_0}{C_t}\right) = k_1 t \tag{2}$$

where C_0 and C_t (μg/L) are the phenanthrene concentrations at time zero and t (min), respectively, and k_0 (μg/(L h)) and k_1 (h^{-1}) are respective rate constants.

2.5. Measurement of hydroxyl radicals (•OH)

The production of hydroxyl radicals (•OH) by various Ti-based materials was measured following the photoluminescence (PL) technique using terephthalic acid as the probe molecule. As terephthalic acid reacts with •OH, 2-hydroxyterephthalic acid will form with a high fluorescent, and the fluorescence intensity is proportional to the amount of •OH. In each test, 0.2 g of a material was dispersed in a mixture of 0.5 mmol terephthalic acid and 2 mmol NaOH with a total volume of 200 mL in the photo-reactor. After 2-h illumination under the solar light, samples were taken and micro-filtered. The PL spectra were then obtained on a fluorescence spectrophotometer (SpectraMax M2, Molecular Devices, CA, USA) at an excitation wavelength of 425 nm.

3. Results and discussion

3.1. Photocatalytic activity of Co-deposited TNTs under different synthesis conditions

Fig. 1 shows photocatalytic degradation of phenanthrene by Co-deposited TNTs prepared with various cobalt loadings and/or at
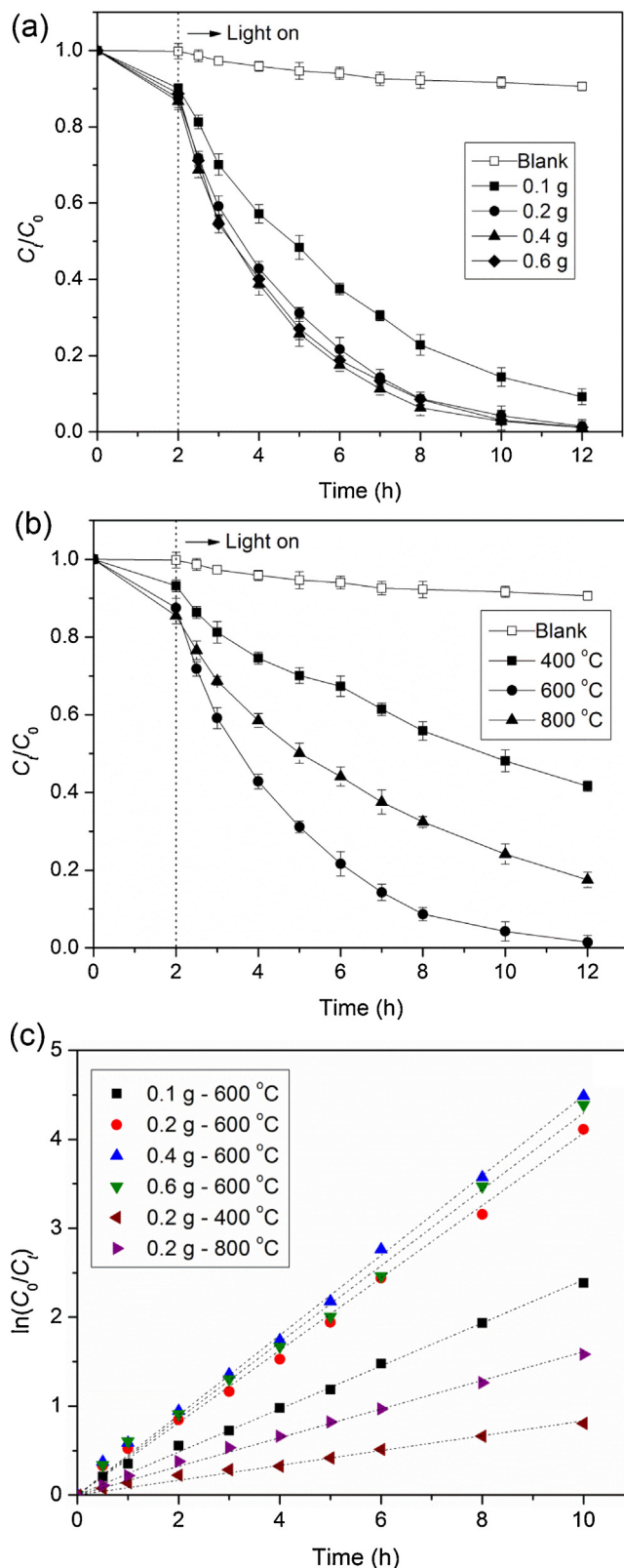

Fig. 1. Photocatalytic degradation of phenanthrene by Co-deposited TNTs synthesized at (a) different Co loadings (but fixed calcination temperature of 600 °C) and (b) various calcination temperatures (but identical Co loading of 2.26%). Lines in (c) are linear first-order model fittings for all the materials (Initial phenanthrene = 200 μg/L, material dosage = 1.0 g/L, pH 7.0 ± 0.2, temperature = 25 ± 0.2 °C).

different calcination temperatures. Table S1 in Supplementary data lists the best fitted parameters for photocatalytic kinetic models. In all cases, the first-order model is able to adequately interpret the kinetic data ($R^2 > 0.98$), with much better fittings than the zero-order model. Fig. 1a shows that increasing the initial $CoCl_2 \cdot 6H_2O$ dosage from 0.1 to 0.2 g in the hydrothermal reaction enhanced the apparent rate constant (k_1) from 0.24 to 0.39 h^{-1}. However, further increasing the cobalt dosage from 0.2 to 0.6 g only modestly affected the k_1 value (0.39 to 0.43 h^{-1}), with nearly the same final phenanthrene removal of >98%. At the initial $CoCl_2 \cdot 6H_2O$ concentrations of 0.1, 0.2, 0.4 and 0.6 g, the Co loadings were (wt%): 1.13, 2.26, 2.68 and 2.81, respectively. Doubling the initial $CoCl_2 \cdot 6H_2O$ from 0.1 to 0.2 g also doubled the Co loading, resulting in 62.5% increase in k_1. However, further increasing $CoCl_2 \cdot 6H_2O$ from 0.2 to 0.6 g resulted in only 0.55 wt% increase in Co loading, and thus, only modest enchantment in the photocatalytic activity.

It is noteworthy that increasing the cobalt dosage from 0.4 to 0.6 g slightly decreased the rate constant from 0.43 to 0.41 h^{-1}, suggesting that there is a limiting value for the Co loading. At lower Co loadings, the deposited Co acts as electron traps that inhibit the recombination of the photo-generated electron-hole pairs; however, when the Co loading dosage exceeds the limit, excessive CoO crystals may facilitate recombination of the electron-hole pairs [42,43], thus reducing photocatalytic activity. Similar results have been reported by previous studies on Cu-deposited titanate nanotubes [42] and Mn-doped titanium nanosheets [43]. The much less further gain in photo-activity can also be due to lowered accessibility of the Co sites upon calcination (see Section 3.2). Based on Fig. 1a, the optimal initial $CoCl_2 \cdot 6H_2O$ dosage was set at 0.2 g.

Increasing the calcination temperature from 400 to 600 °C dramatically increased the k_1 value from 0.083 to 0.39 h^{-1} (by a factor of 4.7). However, the rate was lowered to 0.16 h^{-1} when it was calcined at 800 °C. Calcination temperature is highly related to the crystallinity of materials. Previous studies indicated that increasing the calcination temperature from 400 to 600 °C enhances the crystalline phase of anatase, yet higher temperatures (>700 °C) would cause the formation of rutile, a much weaker photocatalyst than anatase [14,44]. Considering both photocatalytic activity and cost effectiveness, Co-TNTs-600 synthesized with a Co loading (2.26 wt%) and a calcination temperature of 600 °C was chosen as the optimal photocatalyst, which was then fully characterized and studied to elucidate the underlying mechanisms for the enhanced photocatalytic activity.

3.2. Morphology, crystal phases and compositions of Co-deposited TNTs

Fig. 2 shows TEM images of TiO_2, TNTs and Co-TNTs-600. The precursor TiO_2 is present as aggregated particles with a primary particle size range of 20–50 nm (Fig. 2a). Upon the hydrothermal treatment, TiO_2 was transformed into TNTs, which appear as multilayer (4–5 layers) nanotubes, with an inner diameter of ~4.5 nm and outer diameter of ~9 nm (Fig. 2b) [39]. The interlayer distance of the nanotubes is 0.75 nm, which is assigned to the crystal plane of titanate (0 2 0) [38]. When Co-TNTs were calcined at 600 °C, the TNTs were broken into shorter nanotubes with an interlayer distance of 0.68 nm (0 2 0) (Fig. 2c), indicating the high-temperature calcination partly damaged the tubular structure and shrank the interlayer distance. HRTEM images in Fig. S2 indicate part of titanate nanotubes survived the calcination process, though partially broken. In addition, nanoparticles (10–30 nm) with a crystal distance of 0.35 nm were formed, which is in accordance with the crystal plane of anatase (1 0 1) [45]. Furthermore, the calcination resulted in some 2–5 nm nanoparticles (nano-dots) (Fig. 2c), which were further confirmed to be CoO through XRD and XPS analyses. In addition, EDS line-scan of Co-TNTs-600 through section
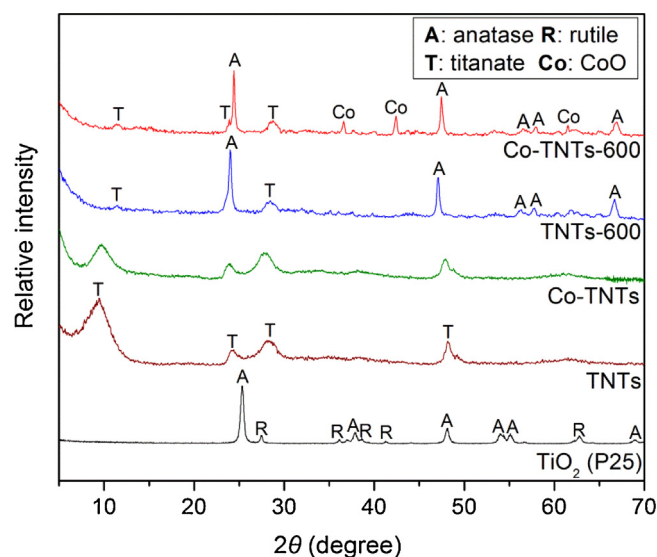

Fig. 3. XRD patterns of various Ti-based materials (TNTs: Titanate nanotubes obtained via hydrothermally treatment of commercial TiO_2; Co-TNTs: Co(II) loaded TNTs; TNTs-600: TNTs calcinated at 600 °C; Co-TNTs-600: Co-deposited TNTs calcinated at 600 °C).

A–A′ (Fig. 2d) shows that the main elements of the new material are Na, O, Ti and Co, indicating successful Co deposition.

Fig. 3 presents the XRD patterns for the materials. The pristine TiO_2 is a mixture of anatase and rutile, which was completely transformed to titanate upon the hydrothermal treatment. The peaks at 10°, 24°, 28° and 48° are all ascribed to sodium titanate [5,46]. The resulting titanate nanotubes are a kind of tri-titanate with a chemical formula of $Na_xH_{2-x}Ti_3O_7$ (x depends on the sodium content) and a skeletal structure of layered corrugated ribbons formed through edge-sharing of triple [TiO_6] octahedrons with H$^+$ and Na$^+$ located in interlayers [5,10,47]. The peak at 10° represents the interlayer distance of TNTs (0.75 nm as shown in Fig. 2b) [5,46]. The XRD patterns for Co-TNTs nearly resemble those of TNTs, indicating that cobalt is loaded as Co(II) ions without formation of crystalline Co oxides in the hydrothermal process, i.e., Co(II) ions substituted Na$^+$ ions in the interlayers of TNTs without altering the titanate lattice. When TNTs are calcinated at 600 °C (TNTs-600), titanate is partially transformed into anatase (peaks at ~25°, 47°, 55°, 58° and 67° JCPDS 21-1272) [48], whereas part of the titanate phase remains as evidenced by the peaks at 10° and 28°. However, the interlayer peak at 10° is greatly weakened due to the breakage of the tubular structure. For Co-TNTs-600, besides the crystal phases of titanate and anatase, a CoO crystal phase arises, as reflected by the peaks at 36.5°, 42.4° and 61.5° (JCPDS 75-0393) [49,50]. Evidently, the calcination converted the interlayered Co(II) into CoO that is deposited in the titanate or formed anatase. The interlayer peak was also observed, though significantly weakened and shifted from 9.5° to 11.3°, which is attributed to the breakage of the tubular and layered structure in the calcination process (Fig. 2c).

Fig. 4 compares the FTIR spectra for the typical Ti-based materials. For TiO_2, the absorption bands at 662, 1633, and 3462 cm^{-1} are attributed to O—H, H—O—H, and Ti—O bonding vibrations [51]. Upon the hydrothermal reaction, two new bands at 480 and 904 cm^{-1} are observed, which are assigned to the [TiO_6] octahedron and the four-coordinated Ti—O stretching vibrations, respectively [5,10,47]. Like the XRD data, the FTIR spectra for TNTs and Co-TNTs are rather alike though the Ti—O band is shifted from 904 to 894 cm^{-1}, which reflects the formation of Ti—O—Co. The FTIR data for TNTs and Co-TNTs confirm the incorporation of Co(II) ions, and the basic skeleton of the [TiO_6] octahedron remains intact during the hydrothermal
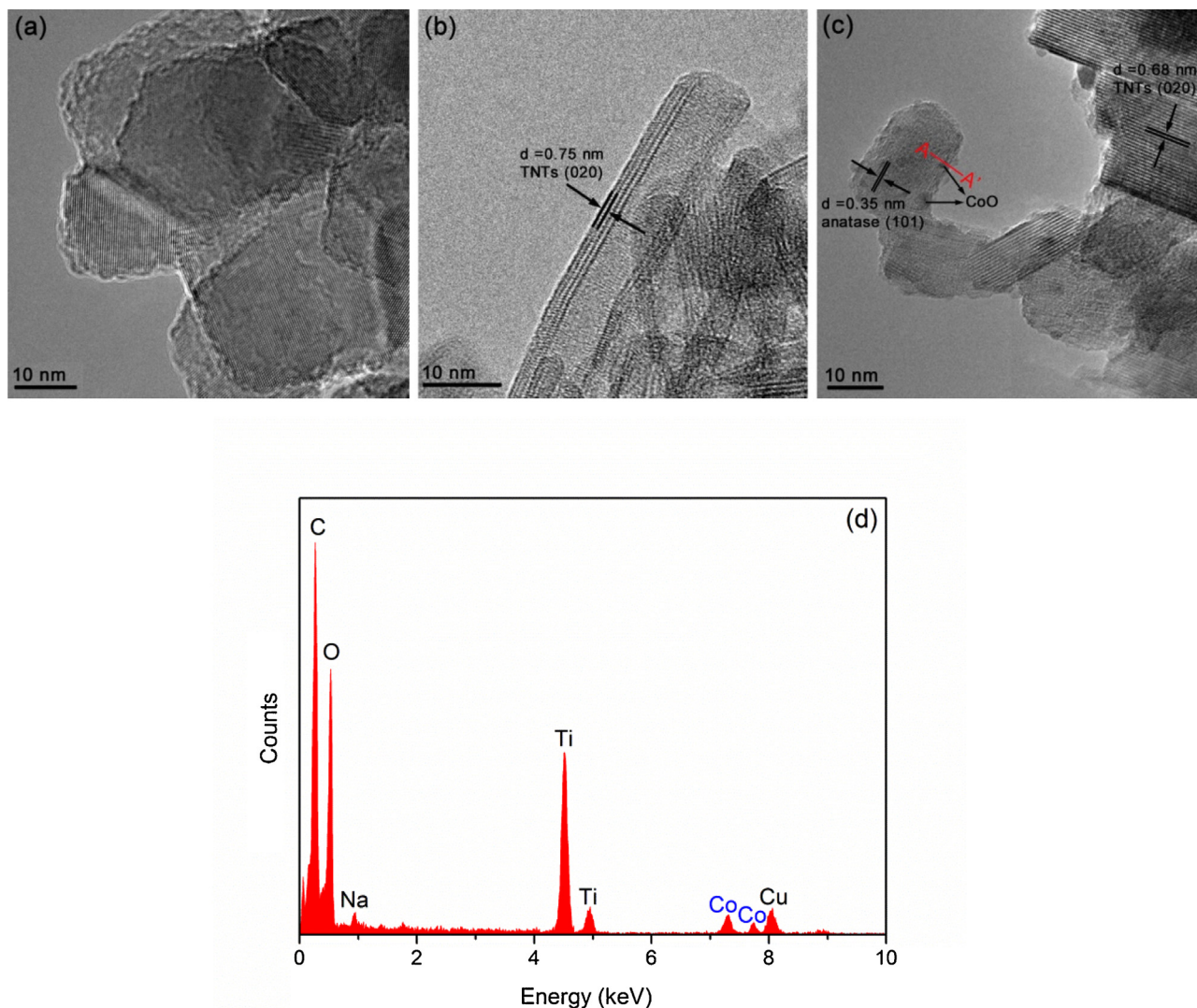
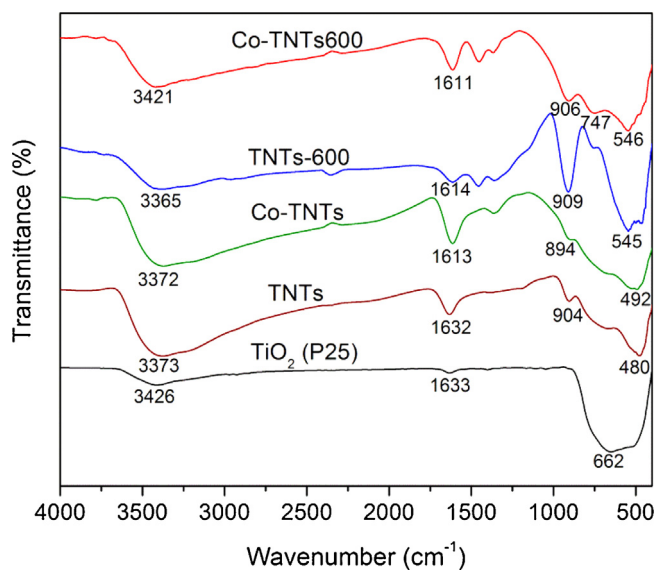**Fig. 2.** TEM images of (a) TiO$_2$ (P25), (b) TNTs, (c) Co-TNTs-600, and (d) EDS spectra of Co-TNTs-600.

Fig. 4. FTIR spectra of various Ti-based materials.

treatment of TNTs. However, when calcined at 600 °C (TNTs-600), the [TiO$_6$] octahedron band shifted to 545 cm^{-1}, indicating the transition of titanate to TiO$_2$ (anatase). For Co-TNTs-600, the new band at 747 cm^{-1} indicates the vibration of Co(II) in the tetrahedral hole (i.e., Co—O) [52], indicating conversion of Co(II) ions into CoO.

Table S2 presents the BET surface area, total pore volume and average pore diameter of P25, TNTs and Co-TNTs-600. Compared to TNTs [10,41,47], the BET surface area and total pore volume of Co-TNTs-600 are decreased from 272.3 m^2 g^{-1} and 1.26 cm^3 g^{-1} for TNTs to 72.5 m^2 g^{-1} and 0.26 cm^3 g^{-1}, respectively, which is due to the collapse of layered tubular structure of TNTs at the calcination temperature. However, the BET surface area and total pore volume of Co-TNTs-600 are still larger than those of P25. The nitrogen adsorption-desorption isotherms with Co-TNTs-600 is aligned with the type IV isotherm with an H3 hysteresis loop according to the BDDT classification (Fig. S3a), indicating mesopores (2–50 nm) are dominant in Co-TNTs-600 [53], which was further confirmed by the pore size distribution (Fig. S3b).

3.3. Photocatalytic degradation of phenanthrene by Co-deposited TNTs

Fig. 5 compares photocatalytic degradation kinetics of phenanthrene by Co-TNTs-600 and other Ti-based materials. Again, the
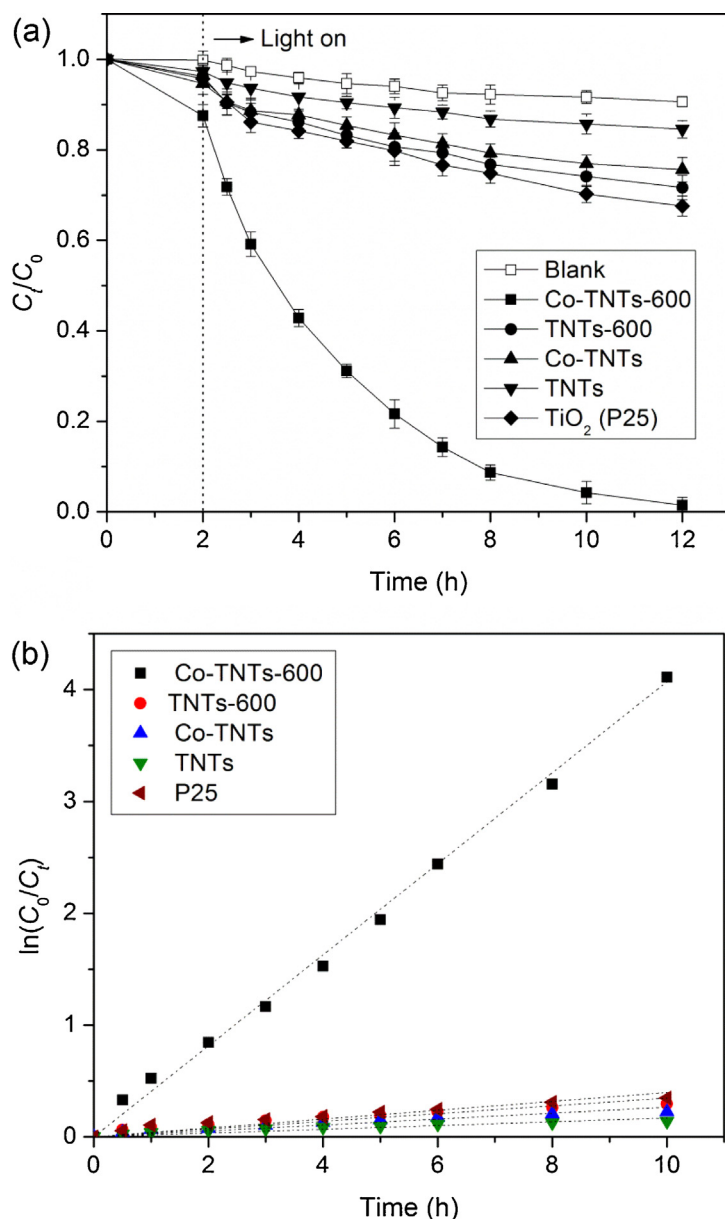
Fig. 5. (a) Photocatalytic degradation of phenanthrene by various Ti-based materials and (b) linear first-order model fitting for the different materials (Initial phenanthrene = 200 μg/L, material dosage = 1.0 g/L, pH = 7.0 ± 0.2, temperature = 25 ± 0.2 °C).

Table 1
Parameters of zero-order and first-order kinetic models for photocatalytic degradation of phenanthrene by different Ti-based materials.

Material	Zero-order model		First-order model	
	k_0 (μg/(L h))	R^2	k_1 (h^{-1})	R^2
Co-TNTs-600	22.91	0.6335	0.39	0.9927
TNTs-600	5.93	0.7581	0.035	0.8266
Co-TNTs	4.58	0.8226	0.027	0.8683
TNTs	3.11	0.7884	0.017	0.8181
TiO$_2$ (P25)	6.63	0.8149	0.040	0.8815

first-order kinetic model is able to better and adequately interpret the photocatalytic reaction kinetics (Table 1). Table 1 gives the resulting parameters of the zero- and first-order kinetic models. In the absence of photodegradation (initial 2 h), Co-TNTs-600 adsorbed 12.5% of phenanthrene (the maximum Langmuir capac-
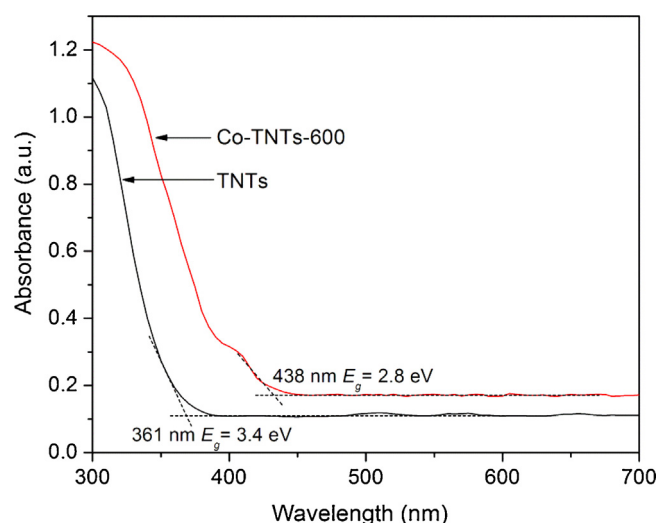

Fig. 6. DRS UV–vis spectra of TNTs and Co-TNTs-600.

ity = 25.8 μg/g, Fig. S4 and Table S3), whereas the other materials adsorbed <6%. Generally, adsorption of phenanthrene is attributed to hydrophobic effects and π–π interactions [54]. Co-TNTs-600 is rather hydrophilic due to the abundant surface −OH groups and inorganic skeleton; hence, it cannot favorably adsorb hydrophobic compounds.

Fig. S5 compares the k_1 values and removal efficiencies (R) for photocatalytic degradation of phenanthrene by different titanium materials. TNTs showed extremely low photocatalytic activity, with a low k_1 of 0.017 h^{-1} and with a phenanthrene removal of 15.5% at 12 h, which is even lower than that of the precursor TiO$_2$ (28.4%). The calcinated TNTs (TNTs-600) increased the removal to 32.5%, whereas deposited Co on TNTs (Co-TNTs, without calcination) increased the removal to 24.4%. However, when Co-deposition and calcination were combined (Co-TNTs-600), the k_1 value was dramatically increased to 0.39 h^{-1} and the removal to 98.6%. The rate constant is ∼23 times that of TNTs and ∼10 times of P25.

Despite the highest specific surface area (Table S2), TNTs showed the lowest photocatalytic activity, which can be attributed to crushing of the TiO$_2$ crystalline, resulting in a high recombination rate of electron-hole pairs after excitation [13–15]. Upon incorporation of Co^{2+} (Co-TNTs), the recombination rate of electron-hole pairs is modestly curbed, resulting in the modest activity increase. The calcination of TNTs (TNTs-600) recovered some of the anatase crystalline (Fig. 3), resulting in a reactivity close to the precursor TiO$_2$. TiO$_2$ and TNTs-600 mainly absorb the UV fraction of the solar light, whereas Co-deposited TNTs facilitate absorption of visible light. Therefore, the combination of Co-deposition and calcination/crystallization resulted in the dramatic synergistic effect of Co-TNTs-600. Upon calcination, the Co(II) ions in TNTs are transformed to Co oxides, which act as electron transfer mediator, inhibiting the hole-electron recombination in the photocatalytic process. In addition, the conversion of titanate anatase crystalline in the calcination process further impedes the electron-hole recombination. Section 3.4 presents more detailed mechanisms on the enhanced photocatalytic activity of Co-TNTs-600.

3.4. Mechanisms for enhanced photocatalytic activity of Co-TNTs-600

Fig. 6 displays the DRS UV–vis spectra of TNTs and Co-TNTs-600. Based on the data, the optical energy gaps for the materials are calculated using Eq. (3) [55]:
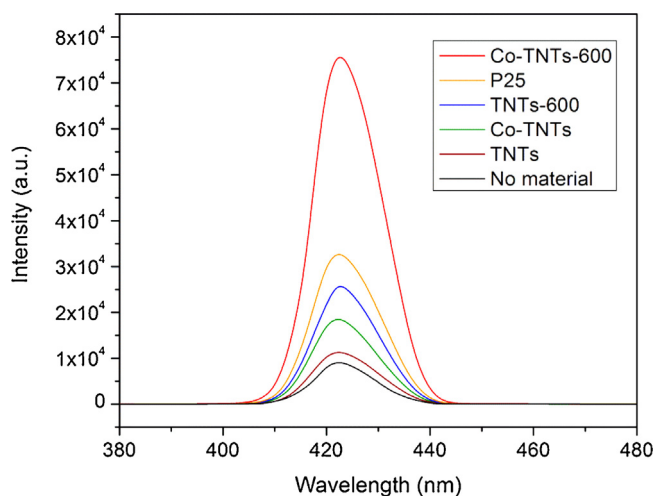
$$\alpha h\nu = A\left(h\nu - E_g\right)^{n/2} \tag{3}$$

Fig. 7. PL spectra of various Ti-based materials under solar irradiation.

in which α, h, ν, A and E_g represent the absorption coefficient, Planck constant, photon frequency, proportionality constant and band gap, respectively; and n is a constant depending on the optical transition type of a semiconductor ($n = 1$ for direct absorption; $n = 4$ for indirect absorption), and $n = 4$ for the titanate materials in this study.
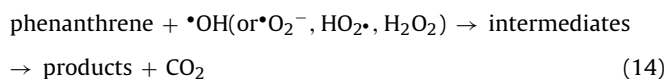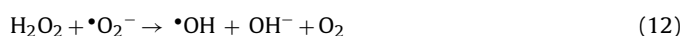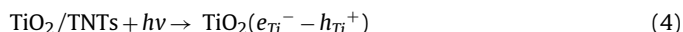
Compared to TNTs, the absorption edge of Co-TNTs-600 shifts to visible region (from 361 to 438 nm), indicating the photo-effect under visible light is enhanced for Co-TNTs-600. The absorbance peak at ca. 430 nm for Co-TNTs-600 can be attributed to the attachment of CoO [50]. The resulting E_g for Co-TNTs-600 is 2.8 eV, compared to 3.4 eV for TNTs and 3.2 eV for P25 [3]. Therefore, a new e-donor level is formed in Co-TNTs-600, which facilitates the transfer of the photo-generated electrons, thereby inhibiting the recombination of the electron-hole pairs.

Fig. 7 shows PL spectra of terephthalic acid, which reflects the production of •OH under solar irradiation. The fluorescence intensity at 425 nm for the materials follows the sequence of: Co-TNTs-600 » P25 > TNTs-600 > Co-TNTs > TNTs, which is consistent with that of the apparent rate constant (k_1) for phenanthrene degradation (Fig. 5 and Table 1). Therefore, enhanced production of the •OH radicals accounts for the enhanced photodegradation of phenanthrene by Co-TNTs-600.

XPS analysis further demonstrates the role of Co in the photocatalysis. As shown in Fig. 8 and Table S4 in Supplementary data, the main elements for TNTs are Na (12.3%), Ti (23.4%) and O (64.3%), with a chemical formula of $Na_{1.58}H_{0.42}Ti_3O_7·1.24H_2O$ based on the basic structure of tri-titanate and interlayered H^+/Na^+. For Co-TNTs-600, a Co 2p peak emerges in the XPS survey spectra (Fig. 8a). The Na content decreases from 12.3% for TNTs to 10.6% for Co-TNTs-600, which is due to the ion exchange of Co^{2+} with Na^+ in the hydrothermal process. The atomic percentage of Co is determined as 1.7% (2.66 wt%) by XPS, which is consistent with the Co loading dosage obtained from the EPA method (2.26 wt%), indicating a relatively low Co-deposition can greatly enhance the photocatalytic activity of TNTs. For the high resolution of O 1s (Fig. 8b), the peaks at ca. 532 eV and 530 eV are assigned to the oxygen from the surface hydroxyl groups and the material lattice, respectively [56]. For TNTs, the oxygen compositions can include O from the surface Ti – OH ($E_b \approx 532$ eV) and the crystal lattice [Ti – O_6] ($E_b \approx 530$ eV) [5]. The lattice O in Co-TNTs-600 is 95.9%, compared to 94.4% for TNTs, indicating transition of titanate to TiO_2 (also see Fig. 3), as the content of hydroxyl groups in TNTs is higher than that in TiO_2 due to the hydrothermal treatment [5,38,39]. In addition, the formation of CoO also leads to the increase of lattice O. For high resolution of

Co 2p (Fig. 8c), the peaks at ca. 796 and 780 eV represent the Co $2p_{1/2}$ and $2p_{2/3}$ orbits, respectively [57,58]. Specifically, the peak at 780 eV is assigned to Co^{2+}, indicating the formation of CoO after calcination [57]. Moreover, there is a satellite Co^{2+} peak at ca. 786 eV, which belongs to Co—O—Ti (Co^{2+} in the interlayers of TNTs) [59]. The resulting CoO accepts the electrons excited by titanate and TiO_2 under visible light, thus inhibiting the recombination of electron-hole pairs.

Fig. 9 illustrates the key mechanisms for the enhanced photocatalytic activity of Co-TNTs-600, and Eqs. (4)–(14) depict the photocatalytic reactions during photocatalytic of phenanthrene. Under illumination of solar light, anatase (the main one), TNTs and CoO all can generate a conduction band (e^-, electrons) and a valence band (h^+, holes) (Eqs. (4)–(5)) [2,23,41,60]. Because the pristine TNTs and TiO_2 are weakly responsive to visible light, the production of the reactive oxygen species (ROS), e.g., •OH, •O_2^-, HO_2•, H_2O_2, will be limited. In addition, the excited electron-hole pairs are prone to recombination for TNTs due to the loss of the crystalline phases. For Co-TNTs-600, however, photo-generated electrons are transferred by CoO coupled with a reduction of Co^{2+} to Co^+ (Eqs. (6)–(7)), thus inhibiting the recombination of electron-hole pairs. Previous studies have confirmed this type of electron transfer mediated by doped/deposited metal oxides, such as CuO, Mn_xO_y, Fe_2O_3 and Co_3O_4 [23,42,43,61]. The electrons can reduce O_2 molecule to •O_2^-, and then produce HO_2• (Eqs. (8)–(9)) [62,63]. In the meanwhile, the holes can oxidize H_2O molecules into the reactive oxygen species (ROS), primarily •OH (Eqs. (10)–(12)) (Fig. 7), which are responsible for phenanthrene degradation (Eqs. (13)–(14)) [32,34,41,63,64]. The cobalt deposition also shifts the light absorption edge to the visible light range and narrows down the energy gap to 2.8 eV, which means there is a new electron acceptor formed (in CoO) acting as photo-generated electrons transfer medium, and therefore, more visible light is absorbed by the new catalyst for photodegradation. Moreover, the rise in anatase crystalline promotes production of more electron-hole pairs under visible light and further impedes the electron-hole recombination.

$$TiO_2/TNTs + h\nu \rightarrow TiO_2(e_{Ti}^- - h_{Ti}^+) \tag{4}$$

$$CoO + h\nu \rightarrow CoO(e_{Co}^- - h_{Co}^+) \tag{5}$$

$$Co(II) + e_{Ti}^- \rightarrow Co(I) \tag{6}$$

$$Co(I) + O_2 \rightarrow Co(II) + •O_2^- \tag{7}$$

$$O_2 + e^- \rightarrow •O_2^- \tag{8}$$

$$•O_2^- + H^+ \rightarrow HO_2• \tag{9}$$

$$H_2O + h^+ \rightarrow •OH + H^+ \tag{10}$$

$$•O_2^- + e^- + 2H^+ \rightarrow H_2O_2 \tag{11}$$

$$H_2O_2 + •O_2^- \rightarrow •OH + OH^- + O_2 \tag{12}$$

$$phenanthrene + h^+ \rightarrow intermediates \rightarrow products + CO_2 \tag{13}$$

$$phenanthrene + •OH(or•O_2^-, HO_2•, H_2O_2) \rightarrow intermediates$$
$$\rightarrow products + CO_2 \tag{14}$$

Figs. S6 and S7 show the total ion chromatograms and the MS spectra of phenanthrene and its photodegradation byproducts at various reaction times, and Fig. 10 decpits the phenantherene degradation pathway in the photocatalytic process using Co-TNTs-600. After 1 h of photo-degradation (Fig. S6b), two main peaks were identified as (1,1-biphenyl)-2,2-dicarboxaldehyde (B) and 9,10-phenanthrenedione (C) (Fig. S7). 9,10-Phenanthrenedione was formed through ketonization of the
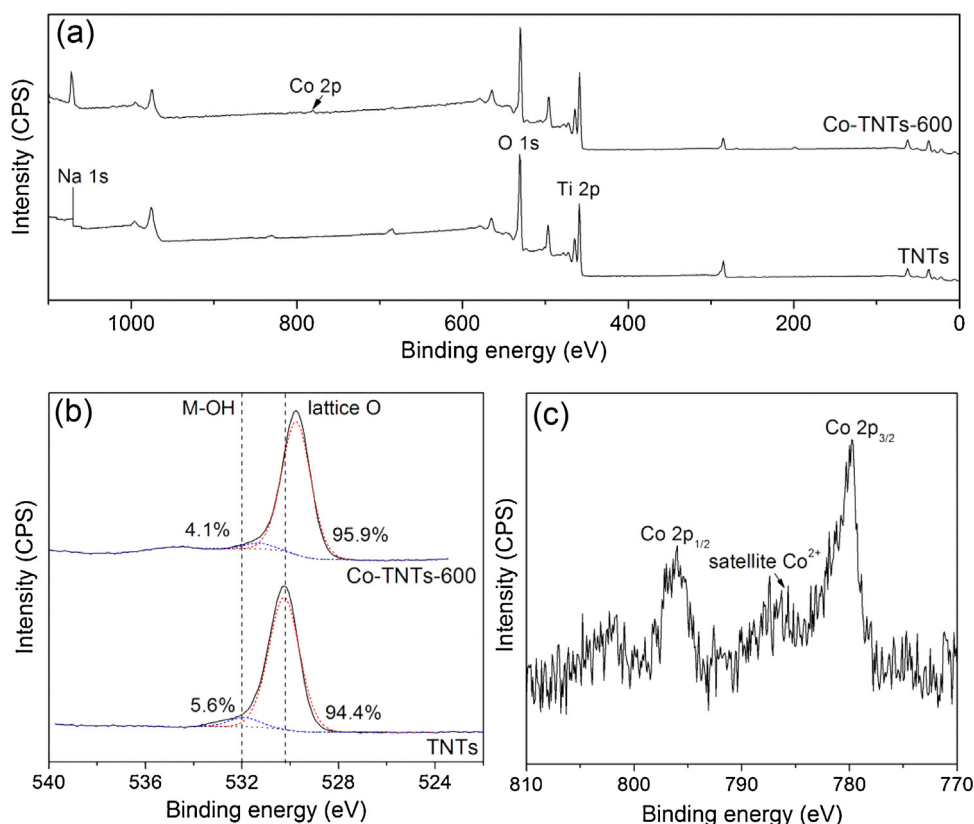
Fig. 8. XPS spectra of TNTs and Co-TNTs-600: (a) Survey, (b) high resolution of O 1s, and (c) Co 2p.

hydroxylated benzene ring of phenanthrene (Steps 1–3 in Fig. 10), and (1,1-biphenyl)-2,2-dicarboxaldehyde was produced via ring-opening of 9,10-phenanthrenedione (Step 4). The results are consistent with those reported by others [34,65,66]. At 3 h (Fig. S6c), 9,10-phenanthrenedione disappeaered while a new peak assigned to bis(2-ethylhexyl) phthalate (D) arose, indicating continued bezene ring opening and subsequent alkylation by some photo-activated alkanes ($\cdot$R) (Steps 6/7-8) [32,34]. At 6 h (Fig. S6d), Product D disappeared, whereas 93% of initial phenanthrene and 27% of (1,1-biphenyl)-2,2-dicarboxaldehyde 1 h were degraded. In the later stage, the phthalates would be further oxidized into smaller organic compounds, such as cyclohexanols, alkanoic acids, alkenes, alkanes, and alcohols (Step 9) [34,65], which are then mineralized to CO_2 and H_2O (Step 10).

3.5. Separation and reuse of Co-TNTs-600

One of the downsides for conventional TiO_2 (especially nano-TiO_2) has been related to poor separation from solutions, which not only limits its use in water treatment, but also prevents from effective recovery of the catalyst. Fig. S8 compares the sedimentation behaviors of Co-TNTs-600 versus P25 and TNTs. In the 180 min of gravity sedimentation, 77.1% of Co-TNTs-600 settled, compared to 64.1% for TNTs and only 0.5% for P25. Over 94% removal of Co-TNTs-600 was achieved in 357 min of sedimentation.

Fig. 11 shows photocatalytic degradation kinetics of phenanthrene by Co-TNTs-600 over 6 cycles of repeated uses, and Table S5 lists the apparent rate constants and the 12-h phenanthrene removal efficiency in each cycle. Evidently, the 12-h phenanthrene removal drops gradually and remains at 87.2% after 6 cycles of operations. In addition, the bleeding of Co from the catalyst totaled at only 4.20% in the 6 runs (2.87% in the first 2 runs) (Table S6), which could be lowered to <0.3% had Co-TNTs-600 been pre-rinsed.
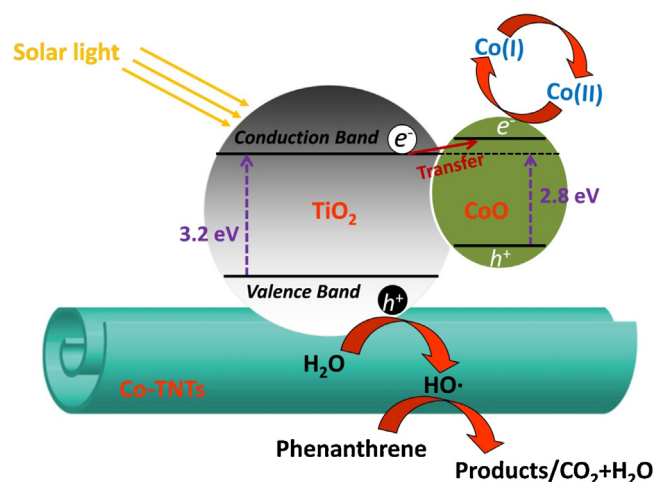
Fig. 9. Schematic illustration of enhanced photocatalytic activity of Co-TNTs-600.

4. Conclusions

This study developed and tested a new class of cobalt-deposited TNTs for enhanced photocatalytic degradation of phenanthrene under solar light. The primary findings are summarized as follows:

(1) Co-deposited TNTs were successfully synthesized through a two-step process, i.e., hydrothermal treatment of commercial P25 as the Ti precursor followed by calcination at 600 °C. Co(II) ions are incorporated in TNTs in the hydrothermal reaction, which are further transformed into CoO in the calcination process. The optimized catalyst (Co-TNTs-600) was prepared at 2.26% Co loading and a calcination temperature of 600 °C. TEM,

Fig. 10. Proposed degradation pathway of phenanthrene by Co-TNTs-600 under solar light.

Fig. 11. Reusing the same Co-TNTs-600 in 6 consecutive runs of photocatalytic degradation of phenanthrene (Initial phenanthrene = 200 μg/L, material dosage = 1.0 g/L, pH = 7.0 ± 0.2, temperature = 25 ± 0.2 °C).

XRD, FTIR and XPS characterizations indicate that Co-TNTs-600 is a nano-composite consisting of titanate, anatase and CoO.

(2) Co-TNTs-600 exhibited high photocatalytic activity for degradation of phenanthrene under solar light, with a 98.6% removal rate in 12 h at dosage of 1 g/L. The first-order kinetic model is able to adequately interpret the kinetic data, and the apparent rate constant was determined to be $0.39\,h^{-1}$, which is ~23 times higher than that of TNTs and ~10 times that of P25. The combination of Co-deposition and calcination/crystallization resulted in the dramatic synergistic effect of Co-TNTs-600.

(3) UV-vis DRS spectra of Co-TNTs-600 suggest that the absorption edge of Co-TNTs-600 shifts to the visible light region compared to P25 and un-calcined TNTs, and Co-TNTs-600 gives a much narrower optical energy gap of 2.8 eV, compared to 3.4 eV for TNTs and 3.2 eV for P25, indicating much improved sensitivity to visible light.

(4) The CoO nanoparticles in Co-TNTs-600 can not only facilitate effective utilization of visible light for production of electron-hole pairs, but also serve as an electron transfer mediator that inhibits recombination of the pairs. Likewise, the anatase crystalline resulting from the calcination process promotes production of more electron-hole pairs and further impedes the electron-hole recombination.

(5) Co-TNTs-600 can be efficiently separated via gravity-settling and then reused in multiple runs.

(6) Despite the much greater catalytic activity of Co-TNTs-600, the photodegradation pathway for phenanthrene appears similar to that for other photocalatlysts. (1,1-biphenyl)-2,2-dicarboxaldehyde and 9,10-phenanthrenedione are the primary intermediates, both of which are expectd to be completely mineralized.

Overall, Co-TNTs-600 appears to be an efficient photocatalyst for degradation of persistent PAHs under solar light.

Acknowledgments

Appendix A. Supplementary data

Supplementary data associated with this article can be found, in the online version, at http://dx.doi.org/10.1016/j.apcatb.2016.01.010.

References

[1] M.A. Shannon, P.W. Bohn, M. Elimelech, J.G. Georgiadis, B.J. Mariñas, A.M. Mayes, Nature 452 (2008) 301–310.
[2] J. Schneider, M. Matsuoka, M. Takeuchi, J. Zhang, Y. Horiuchi, M. Anpo, D.W. Bahnemann, Chem. Rev. 114 (2014) 9919–9986.
[3] X. Chen, C. Burda, J. Am. Chem. Soc. 130 (2008) 5018–5019.
[4] X. Chen, S.S. Mao, Chem. Rev. 107 (2007) 2891–2959.
[5] W. Liu, T. Wang, A.G.L. Borthwick, Y. Wang, X. Yin, X. Li, J. Ni, Sci. Total Environ. 456 (2013) 171–180.
[6] M. Pelaez, N.T. Nolan, S.C. Pillai, M.K. Seery, P. Falaras, A.G. Kontos, P.S. Dunlop, J.W. Hamilton, J.A. Byrne, K. O'Shea, Appl. Catal. B: Environ. 125 (2012) 331–349.
[7] H. Tan, Z. Zhao, M. Niu, C. Mao, D. Cao, D. Cheng, P. Feng, Z. Sun, Nanoscale 6 (2014) 10216–10223.
[8] X. Chen, L. Liu, F. Huang, Chem. Soc. Rev. 44 (2015) 1861–1885.
[9] R. Shankar, W.J. Shim, J.G. An, U.H. Yim, Water Res. 68 (2015) 304–315.
[10] W. Liu, W. Sun, A.G.L. Borthwick, J. Ni, Colloid Surf. A 434 (2013) 319–328.
[11] T. Wang, W. Liu, N. Xu, J. Ni, J. Hazard. Mater. 250 (2013) 379–386.
[12] L. Xiong, W. Sun, Y. Yang, C. Chen, J. Ni, J. Colloid Interface Sci. 356 (2011) 211–216.
[13] S. Kim, M. Kim, S.H. Hwang, S.K. Lim, Appl. Catal. B: Environ. 123 (2012) 391–397.
[14] C.K. Lee, C.C. Wang, M.D. Lyu, L.C. Juang, S.S. Liu, S.H. Hung, J. Colloid Interface Sci. 316 (2007) 562–569.
[15] H. Yu, J. Yu, B. Cheng, M. Zhou, J. Solid State Chem. 179 (2006) 349–354.
[16] C.H. Lin, J.H. Chao, C.H. Liu, J.C. Chang, F.C. Wang, Langmuir 24 (2008) 9907–9915.
[17] J. Yu, H. Yu, B. Cheng, X. Zhao, Q. Zhang, J. Photochem. Photobiol. A 182 (2006) 121–127.
[18] M.A. Khan, H.T. Jung, O.B. Yang, J. Phys. Chem. B 110 (2006) 6626–6630.
[19] K. Chen, L. Zhu, K. Yang, J. Environ. Sci. 27 (2015) 232–240.
[20] Y. Liu, W. Shu, K. Chen, Z. Peng, W. Chen, ACS Catal. 2 (2012) 2557–2565.
[21] H.Y. Chen, S.L. Lo, H.H. Ou, Appl. Catal. B: Environ. 142 (2013) 65–71.
[22] M. Grandcolas, T. Cottineau, A. Louvet, N. Keller, V. Keller, Appl. Catal. B: Environ. 138 (2013) 128–140.
[23] W. Liu, X. Zhao, A.G.L. Borthwick, Y. Wang, J. Ni, ACS Appl. Mater. Interfaces 7 (2015) 19726–19735.
[24] M. Dahl, Y. Liu, Y. Yin, Chem. Rev. 114 (2014) 9853–9889.
[25] R.P. Marin, S.A. Kondrat, J.R. Gallagher, D.I. Enache, P. Smith, P. Boldrin, T.E. Davies, J.K. Bartley, G.B. Combes, P.B. Williams, S.H. Taylor, J.B. Claridge, M.J. Rosseinsky, G.J. Hutchings, ACS Catal. 3 (2013) 764–772.
[26] G. Dai, S. Liu, Y. Liang, T. Luo, Appl. Surf. Sci. 264 (2013) 157–161.
[27] Y.F. Wang, M.C. Hsieh, J.F. Lee, C.M. Yang, Appl. Catal. B: Environ. 142–143 (2013) 626–632.
[28] G. Zhang, H. Huang, W. Li, F. Yu, H. Wu, L. Zhou, Electrochim. Acta 81 (2012) 117–122.
[29] Y. Gong, X. Zhao, Z. Cai, S. O'Reilly, X. Hao, D. Zhao, Mar. Pollut. Bull. 79 (2014) 16–33.
[30] X. Zhao, Y. Gong, S. O'Reilly, D. Zhao, Mar. Pollut. Bull. 92 (2015) 160–169.
[31] J.J. Nam, G.O. Thomas, F.M. Jaward, E. Steinnes, O. Gustafsson, K.C. Jones, Chemosphere 70 (2008) 1596–1602.
[32] S. Wen, J. Zhao, G. Sheng, J. Fu, P.a. Peng, Chemosphere 46 (2002) 871–877.
[33] J. Kou, H. Zhang, Y. Yuan, Z. Li, Y. Wang, T. Yu, Z. Zou, J. Phys. Chem. C 112 (2008) 4291–4296.
[34] H. Jia, J. Zhao, X. Fan, K. Dilimulati, C. Wang, Appl. Catal. B: Environ. 123–124 (2012) 43–51.
[35] W. Sirisaksoontorn, S. Thachepan, A. Songsasen, J. Environ. Sci. Health Part A 44 (2009) 841–846.
[36] C. Wangl, A. Yediler, A. Peng, A. Kettrup, Chemosphere 30 (1995) 501–510.
[37] United States Environment Protection Agency (USEPA). In Acid Digestion of Sediments, Sludges, and Soils, Method 3050B, Revision 2, Washington, DC, USA (1996).
[38] Q. Chen, W.Z. Zhou, G.H. Du, L.M. Peng, Adv. Mater. 14 (2002) 1208–1211.
[39] L. Xiong, Y. Yang, J. Mai, W. Sun, C. Zhang, D. Wei, Q. Chen, J. Ni, Chem. Eng. J. 156 (2010) 313–320.
[40] H. Al-Ekabi, N. Serpone, J. Phys. Chem. 92 (1988) 5726–5731.
[41] W. Liu, J.R. Ni, X.C. Yin, Water Res. 53 (2014) 12–25.
[42] R.A. Doong, S.M. Chang, C.W. Tsai, Appl. Catal. B: Environ. 129 (2013) 48–55.
[43] D.Z. Lu, P.F. Fang, X.Z. Liu, S.B. Zhai, C.H. Li, X.N. Zhao, J.Q. Ding, R.Y. Xiong, Appl. Catal. B: Environ. 179 (2015) 558–573.
[44] J.G. Yu, H.G. Yu, B. Cheng, C. Trapalis, J. Mol. Catal. A: Chem. 249 (2006) 135–142.
[45] J. Zhang, Y. Zhang, Y. Lei, C. Pan, Cata. Sci. Technol. 1 (2011) 273–278.
[46] X.M. Sun, Y.D. Li, Chem. Eur. J. 9 (2003) 2229–2238.
[47] L. Xiong, C. Chen, Q. Chen, J. Ni, J. Hazard. Mater. 189 (2011) 741–748.
[48] M. Choi, K. Yong, Nanoscale 6 (2014) 13900–13909.
[49] R. Qiao, X.L. Zhang, R. Qiu, J.C. Kim, Y.S. Kang, Chem. Eur. J. 15 (2009) 1886–1892.
[50] X. Zheng, G. Shen, Y. Li, H. Duan, X. Yang, S. Huang, H. Wang, C. Wang, Z. Deng, B.L. Su, J. Mater. Chem. A 1 (2013) 1394–1400.
[51] O.K. Park, Y.S. Kang, Colloids Surf. A 257–58 (2005) 261–265.
[52] H.K. Lin, H.C. Chiu, H.C. Tsai, S.H. Chien, C.B. Wang, Catal. Lett. 88 (2003) 169–174.
[53] S. Brunauer, L.S. Deming, W.E. Deming, E. Teller, J. Am. Chem. Soc. 62 (1940) 1723–1732.
[54] W. Chen, L. Duan, D. Zhu, Environ. Sci. Technol. 41 (2007) 8295–8300.
[55] C. Feng, F. Teng, Z. Liu, C. Chang, Y. Zhao, S. Wang, M. Chen, W. Yao, Y. Zhu, Appl. Catal. A: Chem. 401 (2015) 35–40.
[56] H.H. Ou, C.H. Liao, Y.H. Liou, J.H. Hong, S.L. Lo, Environ. Sci. Technol. 42 (2008) 4507–4512.
[57] P. Konova, M. Stoyanova, A. Naydenov, S. Christoskova, D. Mehandjiev, Appl. Catal. A: Gen. 298 (2006) 109–114.
[58] S. Wang, P. Li, H. Liu, J. Li, Y. Wei, J. Alloy. Compd. 505 (2010) 362–366.
[59] V.A. de la Pena O'Shea, M.C. Alvarez Galvan, A.E. Platero Prats, J.M. Campos-Martin, J.L.G. Fierro, Chem. Commun. 47 (2011) 7131–7133.
[60] L. Liao, Q. Zhang, Z. Su, Z. Zhao, Y. Wang, Y. Li, X. Lu, D. Wei, G. Feng, Q. Yu, X. Cai, J. Zhao, Z. Ren, H. Fang, F. Robles-Hernandez, S. Baldelli, J. Bao, Nat. Nanotechnol. 9 (2014) 69–73.
[61] Y. Brik, M. Kacimi, M. Ziyad, F. Bozon-Verduraz, J. Catal. 202 (2001) 118–128.
[62] H. Kaczmarek, L.Å. Lindén, J.F. Rabek, Polym. Degrad. Stabil. 47 (1995) 175–188.
[63] A.L. Linsebigler, G.Q. Lu, J.T. Yates, Chem. Rev. 95 (1995) 735–758.
[64] Y. Zhang, Z. Jiang, J. Huang, L.Y. Lim, W. Li, J. Deng, D. Gong, Y. Tang, Y. Lai, Z. Chen, RSC Adv. 5 (2015) 79479–79510.
[65] J. Kou, Z. Li, Y. Yuan, H. Zhang, Y. Wang, Z. Zou, Environ. Sci. Technol. 43 (2009) 2919–2924.
[66] O.T. Woo, W.K. Chung, K.H. Wong, A.T. Chow, P.K. Wong, J. Hazard. Mater. 168 (2009) 1192–1199.